CHAPTER 3

SYNTHESES AND CHARACTERIZATION OF MO$_X$ (M = Mo, W AND V) NANORODS AND MS$_2$ (M=Mo AND W) NANOSTRUCTURES

3.1 Introduction

Several synthetic approaches including electrochemical techniques, sonochemical approach, template mediated synthesis, bioligation, hydrothermal, wet organic and inorganic routes and thermal methods have been reported to fabricate 1D tungsten oxide nanostructures such as nanorods and nanowires (Polleux *et al.*, 2005 & 2006; Lee *et al.*, 2003; Wang *et al.*, 2006; Li *et al.*, 2003a; Liu *et al.*, 2003). Growth of WO$_{3-x}$ nanorods on the tips of electrochemically etched tungsten filament was achieved by heat treatment of the tips in Ar and H$_2$ atmosphere (Gu *et al.*, 2002; Zhang *et al.*, 2004). However, synthesis of such structure has been possible only in the presence of H$_2$ atmosphere. The nanorods of WO$_3$ have also been obtained by sonochemical method wherein Koltypin *et al.* have synthesized a mixture of WO$_2$-WO$_3$ nanorods by ultrasound irradiation of W(CO)$_6$ in diphenylmethane (Koltypin *et al.*, 2002). Tungsten oxide nanorods could also be obtained from templated route by using CNTs and colloidal gas aphrons as templates (Satishkumar *et al.*, 2000; Shankar *et al.*, 2006; Abdullah *et al.*, 2006). Therese *et al.*, (2005) have adopted an organic amine assisted low temperature hydrothermal route for the synthesis of hexagonal WO$_3$ nanorods. Inorganic compounds such as Na$_2$SO$_4$, Rb$_2$SO$_4$ and K$_2$SO$_4$ have been demonstrated as structure directing agents for the hydrothermal synthesis of 1-D WO$_3$ nanorods (Lou and Zeng, 2003; Gu *et al.*, 2006; Xiao *et al.*, 2007). Srivastava *et al.*, (2006) have reported sol-gel method followed by dip coating to produce WO$_3$ nanorods. By altering the composition and concentration of solvent, it was shown

1

that different morphologies and phases of WO_3 nanorods can be achieved (Choi *et al*., 2005). A combination of sol-gel and alumina membrane as template has been reported for the synthesis of nanofibrils of WO_3 (Lakshmi *et al*., 1997). But, the method produces fibrils that are found to have a diameter and length of 200 nm and 50μm respectively and this is beyond the nanoregime. All of these reported efforts involve multistep processes and limited to the use of directing agents such as CNTs and M_2SO_4 (M=Na, Rb and K). Hence, the synthesis would be tedious and requires careful removal of the structure directing agents to avoid contaminants. Moreover, sol–gel and hydrothermal methods proceed with a low yield. In order to overcome the difficulties mentioned, thermal method has been employed widely for the large scale synthesis of tungsten oxide nanorods/nanowires as they are simple, easy and free from catalysts and contaminants. Heat treatment of tungsten metal, such as, tungsten foil, tungsten wire or tungsten filament heated at 800 – 1600 °C (Guo *et al*., 2004; Shingaya *et al*., 2004; Rothschild *et al*., 2000, Liu *et al*., 2003; Klinke *et al*., 2005; Li *et al*., 2003b), tungsten powder heated at 950 °C under the Ar gas flow on ITO glass/tungsten substrate at 900 -1100 °C (Liao *et al*., 2006), thermal evaporation of tungsten or tungsten oxide powder (Baek *et al.,* 2006; Baek and Yong, 2007), sublimation of WO_3 thin layer deposited on a mica substrate (Gillet *et al*., 2005a & b) and tungsten hexacarbonyl heated at 700 °C (Park and Yong, 2005) have yielded 1-D WO_3 nanorods. All the above thermal methods related to 1-D tungsten oxide formation from the gaseous phase (vapor deposition) or thermal evaporation techniques are technically complex, require high temperature, harsh growth conditions, expensive experimental setup and complicated control processes. Recently, the single source molecular precursor route has opened a useful way for the synthesis of WO_3 nanorods/nanowires by thermal decomposition method (Li *et al*.,

2002; Li *et al.*, 2003; Pol *et al.*, 2005). It offers the distinct advantage of simplified fabrication procedure and equipment as compared with the thermal evaporation or vapor deposition methods. However, multiple steps for the synthesis of both precursor and 1-D WO_3, longer reaction time for precursor (6 days or 10h) and relatively higher pyrolysis temperature (750 °C) were required.

Nanostructures of molybdenum oxides in various forms were synthesized by solution method, by direct oxidation of Mo with and without catalysts at ambient temperature, electrodeposition, thermal evaporation and hydrothermal synthesis. Zhou *et al.* (2003a &b) have grown MoO_2 nanowire arrays on Si substrate by heating a Mo boat to ~1100° C under a constant flow of argon for 60 min in a vacuum chamber. Further heat treatments to reduce or oxidize the obtained MoO_2 nanowires were carried out at different atmosphere and temperature to yield Mo and MoO_3. The field emission properties have been investigated and it has been shown that the MoO_2 nanowires exhibited better field emission properties than those of many other nanomaterials and hence constitute better candidate for vacuum microelectronic devices. Satishkumar *et al* (2000) have synthesized MoO_2 nanorods by the reduction of MoO_3 nanorods at 500° C for 48h where the MoO_3 nanorods were obtained by carbon nanotubes templated growth. However, the time required is long and also the diameter (150-300 nm) of the MoO_2 nanorods is beyond the nano regime i.e., above 100 nm. Zach *et al.*, (2000 & 2002) have employed ESED (electrochemical step edge decoration) method to form MoO_2 nanowires on a highly oriented pyrolytic graphite (HOPG) and the method involves electrochemical deposition of MoO_2 from aqueous sodium molybdate solution. The deposited MoO_2 can also be easily removed from the graphite. In this method, MoO_2 has been used as the precursor to form metallic Mo on HOPG. Bowler *et al.,* (2005) have also adopted the electrochemical deposition

method to form MoO_2 nanowires on HOPG. Ma *et al.*, (2006) have followed thermal evaporation technique where Mo filaments where heated to ~1200° C for 30 min at a pressure of ~ 10 Torr to form MoO_2 nanorods on Si wafers. Magnetic properties of the MoO_2 nanorods were studied and it revealed that they become soft magnetic materials at 10K, implying that the structural or magnetic transition occur at 10K. Molybdenum wire in the form of a spiral coil kept in a vacuum chamber was heated by applying voltage to deposit MoO_2 nanorods on a Si substrate (Liu *et al.*, 2004 and Kumari *et al.*, 2007). Synthesis of molybdenum oxide nanoparticles coated with carbon (MoO_2/C) was carried out by Reaction under Autogenic Pressure at Elevated Temperature (RAPET) reaction at 700 °C for 3h using $MoO(OMe)_4$ as the precursor compound and to obtain the separated molybdenum oxide nanoparticles and carbon, a static magnetic field of 10 T was applied. (Pol *et al.*, 2004). However, the method has not produced 1-D MoO_2 eventhough by using similar strategy 1-D WO_3 could be obtained. Hydrothermal treatment of ammonium molybdate with different surfactants followed by heat treatment at 400 C in Ar atmosphere for 6h yielded MoO_2 with different morphologies resulting in zero, one and two dimensional nanomaterials (Liang *et al.*, 2006a). The same group has also continued to study the Li intercalation behavior of the materials (Liang *et al.*, 2006b).

Among the metal chalcogenides, syntheses of MoS_2 and WS_2 nanomaterials find significance as they exhibit several applications such as catalysts (Cheng *et al.*, 2006), electrochemical hydrogen storage devices (Cheng and Chen, 2006), materials for batteries (Dominko *et al.*, 2003), lubricants (Rapport *et al.*, 2005) and tips for scanning probe microscopes (Rothschild *et al.*, 1999). The syntheses of inorganic counterparts of carbon fullerenes and carbon nanotubes based on early transition metal chalcogenides were first reported by Tenne *et al.*, (1992), followed by several other groups (Remskar *et al.*, 1996; Remskar *et al.*, 2001; Margulis *et al.*, 1993). The

4

syntheses of MoS_2 and WS_2 nanotubes were carried out by treating the metal oxides in an atmosphere of forming gas (95% N_2 + 5% H_2), followed by heating in a stream of H_2S at elevated temperature with the production of considerable amounts of MoS_2 and WS_2 fullerenes (Feldman *et al.*, 1995). In this method, the oxides are initially reduced to their suboxides, followed by their conversion to sulfides. Later, it has been shown that WS_2 nanotubes can also be synthesized by treating WO_{3-x} nanowhiskers precursors in H_2S atmosphere (Rothschild *et al.,* 2000). In the methods above, metal oxides on treatment with H_2S produces metal trisulfides as the intermediate which then loses sulfur on annealing and crystallizes in the form of a disulfide nanotube or nanoparticle. Following this idea, metal sulfide nanotubes were also synthesized by employing sulfides as starting materials. By using ammonium thiomolybdates, such as $(NH_4)_2MoS_4$ and $(NH_4)_2Mo_3S_{13}$ as precursors and aluminium oxide membrane as template, thermal decomposition was carried out to obtain nanofibers and nanotubules of MoS2 (Zelenski and Dorhout, 1998). Thermal decomposition of $(NH_4)_2MoS_4$ at 400 °C in an argon atmosphere was carried out to produce molybdenum trisulfides, which is then heated in a stream of H_2 at 1200-1300 °C to yield MoS_2 nanotubes (Nath, *et al*., 2001; Gloskovskii *et al*., 2006). Tian *et al*., (2004) have reported the syntheses of nanorods and nanotubes of MoS_2 by a hydrothermal treatment using MoO_3 and KSCN as starting materials. Hydrothermal treatment of amine intercalated Li_xMoS_2 lamella was reported for the synthesis of nanocoils and nanotubes of MoS_2 (Lavayen *et al*., 2007). MoO_3 or WO_3 nanorods have been used as precursors for the synthesis of MoS_2 or WS_2 by hydrothermal method (Lou and Zeng, 2002; Therese *et al*., 2005). Template method has also been reported for the synthesis of nanotubes of MoS_2 by using alumina membrane (Santiago *et al.*, 2004).

3.1.1 Mechanism for the formation of MS$_2$ from their oxides

The syntheses of metal sulfides from their respective trioxides have been reported for the synthesis of various nanostructures of molybdenum sulfides and tungsten sulfides. In all these reports, the sulfides are synthesized by heating the metal oxides first in a flowing H$_2$/N$_2$ atmosphere mixture and then in flowing H$_2$S gas (Rothschild *et al*., 2000; Feldman *et al*., 1996). In the current study too, similar strategy has been adopted but the oxides are not taken as the starting materials but they are produced during the process. The synthesis of molybdenum or tungsten sulfide from the tetrabutylammonium molybdate or tungstate proceeds via the formation of oxide, followed by the treatment with H$_2$S gas. Hence the reported mechanism for the sulfide formation from oxides hold good in this case too. According to the reports, the starting material, an oxide nanoparticle, reacts with the H$_2$S gas, which leads to the growth of a complete sulfide shell engulfing the entire oxide nanoparticle. Within a very short time hydrogen diffusion into (and oxygen diffusion out of) the nanoparticles lead to reduction of the oxide core. In the next stage of the reaction, sulfur diffuses into the core and slowly converts the remaining oxide into sulfide, which becomes hollow at the end of the process.

In the present study, syntheses of one-dimensional nanorods of metal oxides such as tungsten trioxides, molybdenum dioxides and mixed oxides of molybdenum and vanadium were carried out. The reactions were further continued by heat treatment of the obtained oxides in the H$_2$S atmosphere to give nanomaterials of metal sulfides such as tungsten disulfide and molybdenum disulfide.

3. 2 Experimental

3.2.1 WO$_3$ nanorods

Tungsten trioxide nanorods have been synthesized by using tetrabutylammonium decatungstate as the precursor material. The starting material was prepared according to the work described elsewhere (Chemseddine *et al*., 1984). The typical procedure involved the precipitation of tetrabutylammonium decatungstate by adding an aqueous tetrabutyl ammonium bromide solution to a clear yellow solution of tungstic acid preformed using sodium tungstate and concentrated hydrochloric acid. The white precipitate was washed with boiling water and ethanol, filtered, dried and then recrystallized in hot dimethyl formamide to give yellow crystals. The thermogravimetric analysis revealed that the tetrabutylammonium cation content in the compound is 29.0% (theoretical value: 29.2%) and the decomposition temperature is around 450° C as reported (Chemseddine *et al*., 1984). The synthesis of tungsten trioxide (WO$_3$) nanorods from tetrabutylammonium decatungstate (($(C_4H_9)_4N)_4W_{10}O_{32}$) was carried out as follows: The precursor compound (1 g) was taken in an alumina or quartz boat and loaded inside a tubular furnace and heated at 450° C at a heating rate of 25° C per min under Ar atmosphere for 3 h. This was followed by gradual cooling to room temperature to obtain a blue powder of WO$_3$ nanorods. The total yield of the obtained material was 71% by weight (relative to the starting material). To further investigate the role of tetrabutylammonium (TBA) group on the morphology of WO$_3$, an experiment was carried out in the absence of tetrabutylammonium ion. To achieve this, $(NH_4)_{10}H_2W_{12}O_{42}.xH_2O$ was taken as the precursor and pyrolysed under similar experimental conditions that were employed for the formation of WO$_3$ nanorods.

3.2.2 MoO$_2$ nanorods

Tetrabutylammonium hexamolybdate ($((C_4H_9)_4N)_2Mo_6O_{19}$ was used as the precursor material for the synthesis of MoO$_2$ nanorods. The precursor material was synthesized as described elsewhere (Che *et al*., 1979). In a typical procedure, acetic anhydride was added to sodium molybdate stirred in dimethyl formamide, followed by acidification with concentrated hydrochloric acid, resulting in heating of the solution. The hot solution was filtered and the yellow filtrate was precipitated with a solution of tetrabutylammonium bromide in dimethylformamide. The resulting salt was filtered, washed with ethanol and ether, and finally recrystallized from acetone. The resultant precursor was taken in a quartz boat and introduced inside a tubular furnace and heated at 400° C at a heating rate of 25° C per min under Ar atmosphere for 3 h. This was followed by gradual cooling to room temperature to obtain the MoO$_2$ nanorods.

3.2.3 Mo$_x$V$_y$O$_z$ nanorods

The nanorods of Mo$_x$V$_y$O$_z$ were prepared by the thermal decomposition of $(Bu_4N)_4[PMo_{10}V_2O_{40}]$. The precursor was prepared as described by Nomiya *et al*., (1997). The method involved a simple precipitation in which 10-Molybdo-2-vanadophosphoric acid ($H_5[PMo_{10}V_2O_{40}]$. $14H_2O$) and tetrabutyl ammonium bromide (Bu_4NBr) were used as the starting materials (Tsigdinos and Hallada, 1968). The orange solid formed was filtered and washed with water and then dried in a vacuum desiccator.

3.2.4 MoS$_2$ nanomaterials

The synthesis of MoS$_2$ nanomaterials was achieved from the tetrabutylammonium hexamolybdate as the precursor via the formation of MoO$_2$ nanorods. The precursor, tetrabutylammonium hexamolybdate was taken in a quartz tube and loaded inside a tubular furnace and heated at 400° C in N$_2$ atmosphere for 3h. It was then followed

by heating at 550 ° C in H_2S atmosphere for 1h. It was then gradually cooled to room temperature to obtain the nanomaterials of molybdenum sulfide.

3.2.5 WS$_2$ nanomaterials

The synthesis of WS$_2$ nanomaterials have been achieved from the tetrabutylammonium hexamolybdate as the precursor via the formation of WO$_3$ nanorods. The precursor, tetrabutylammonium decatungstate was taken in a quartz tube and loaded inside a tubular furnace and heated at 450° C in N_2 atmosphere for 3h. It was then followed by heating at 750 ° C in H_2S atmosphere for 1h. It was then gradually cooled to room temperature to obtain the nanomaterials of tungsten sulfide.

3. 3 Characterization of WO$_3$ nanorods

3.3.1 TGA analysis of (($C_4H_9)_4N)_4W_{10}O_{32}$)

Thermogravimetric analysis (Fig. 3.1) of tetrabutylammonium decatungstate (under Ar atmosphere at a scan rate of 10° C per min) shows a two step decomposition process in the region 300 -410° C. A total weight loss of 29% (calculated value: 29.2%) has been observed and this corresponds to the weight of tetrabutylammonium group. Hence the two step decomposition can be attributed to stepwise decomposition of tetrabutyl ammonium cation of the salt. The percentage of remaining mass is 71%, which corresponds to 10 WO$_3$. This infers that at 450 °C, the cation have decomposed off from the precursor leading to the formation of tungsten trioxide nanorods.
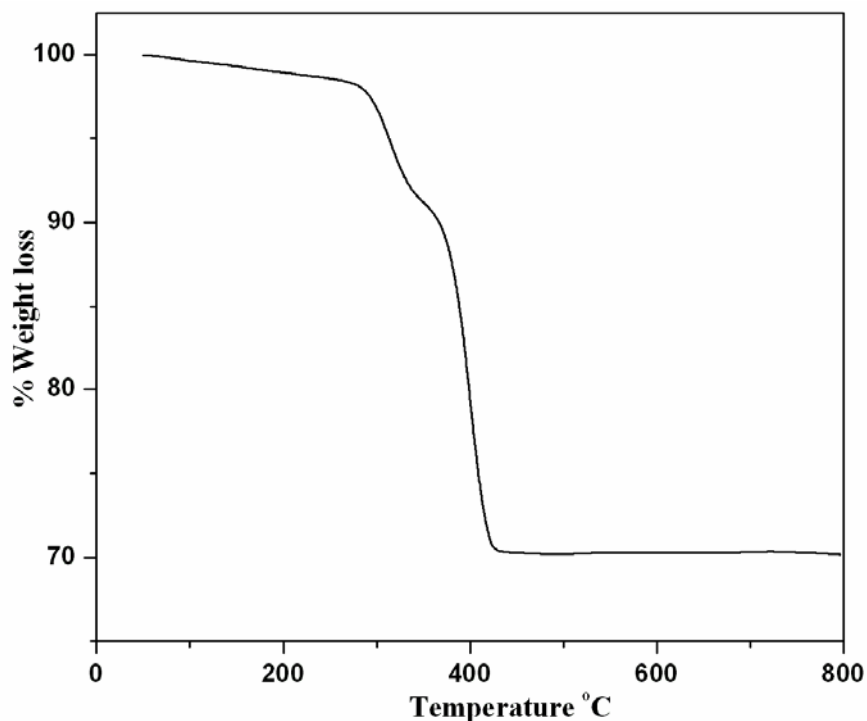
Fig. 3. 1 Thermogravimetric analysis of the precursor, tetrabutylammonium decatungstate

3. 3. 2 X-ray diffraction studies

Fig. 3.2 shows the XRD recorded for WO_3 nanorods synthesized by a single step pyrolysis of tetrabutylammonium decatungstate. All the peaks can be undisputedly indexed to monoclinic WO_3 (JCPDS: 75–2072). There are no peaks detected for other phases, indicating that single phase of WO_3 with high purity has been prepared. The average crystallite sizes of the nanorods was calculated by using Scherrer's formula

$$L = 0.89\,\lambda\,/\,\beta\cos\theta,$$

where, L is the average crystallite size, $\lambda = 0.15418$ nm for CuK_α, β is the half maximum peak width and θ is the diffraction angle in degrees. The average crystallite size values calculated along the (001), (020), (200), (021) and (220) planes have been found to be about 36, 27, 34, 39 and 33 nm, respectively.
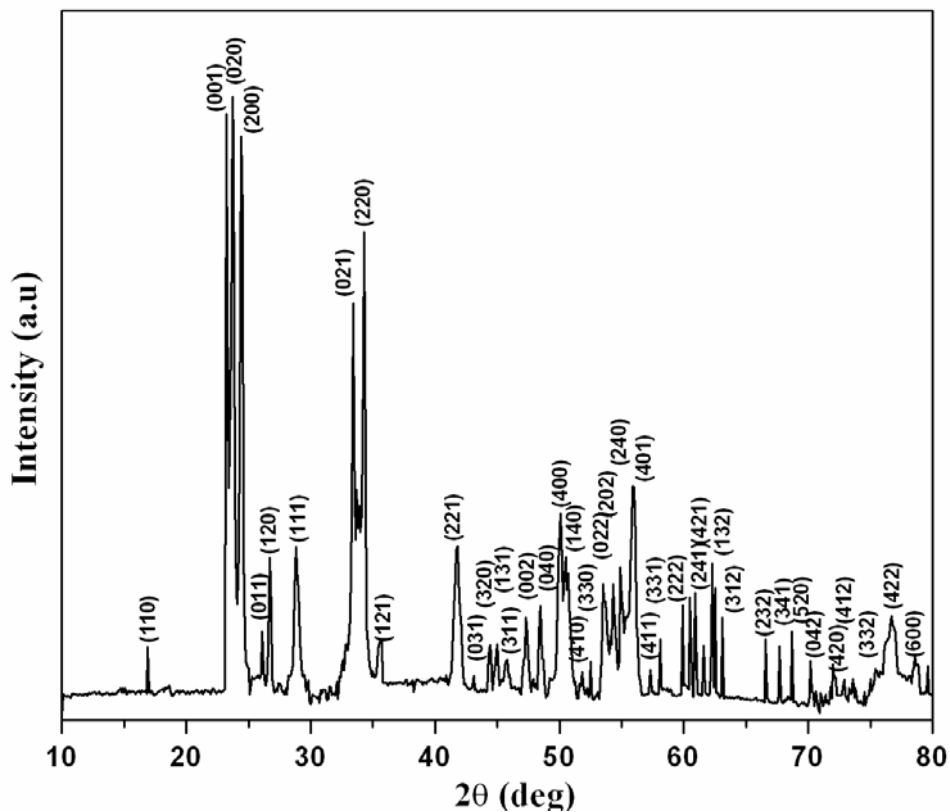
Fig. 3. 2 X-ray diffraction pattern of WO_3 nanorods

3. 3. 3 Raman analysis

The micro-Raman spectrum of the WO_3 nanorods (Fig. 3.3) shows well defined Raman bands at 269, 329, 703 and 813 cm^{-1}. These bands match well with the fundamental modes of monoclinic WO_3 as reported earlier (Santato *et al*., 2001). The Raman spectrum for the material shows characteristic O–W–O bending (259 and 334 cm^{-1}) and the respective stretching modes (703 and 813 cm^{-1}) of WO_3.
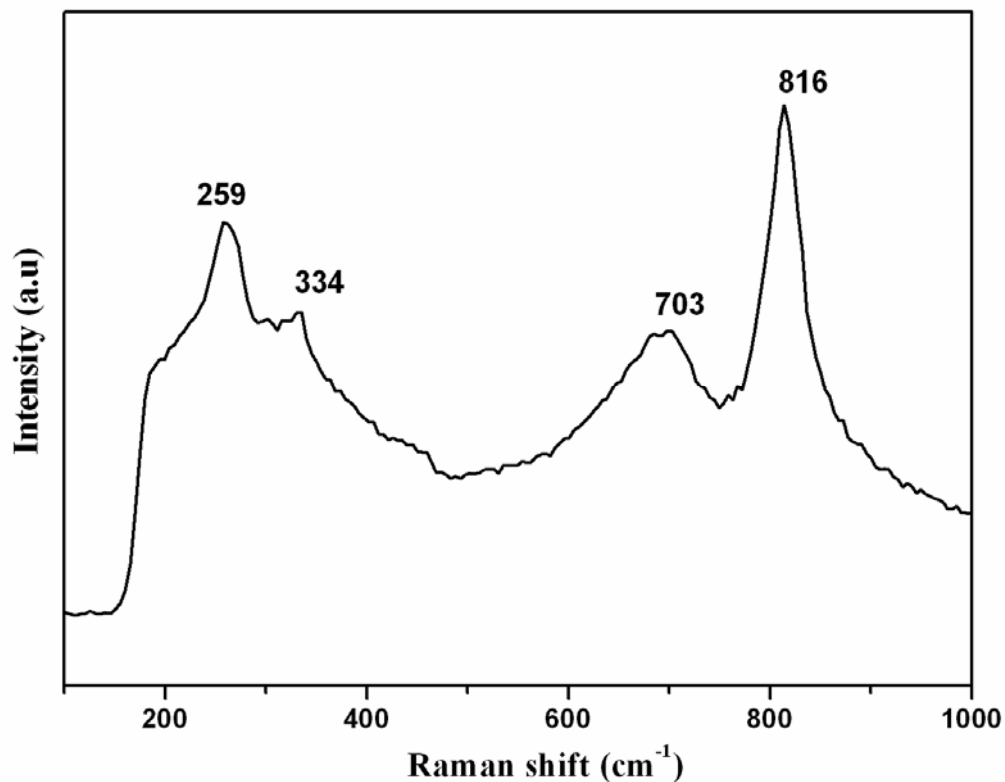
Fig. 3. 3 Raman spectrum of WO_3 nanorods

3. 3. 4 SEM characterization

The typical images of the precursor compound, tetrabutylammonium decatungstate, $((C_4H_9)_4)N)_4W_{10}O_{32}$ and the as synthesized WO_3 are presented in Fig. 3. 4a and b respectively. Fig 3.4a displays the side view of the precursor compound revealing a lamellar aggregation. Fig 3.4b presents the image of the as synthesized WO_3 showing the formation of nanorods in high yields. A magnified image of this has been given in Fig. 3.4c which clearly shows the rod like morphology of the as-synthesized WO_3. The rods are polydispersed with a few hundred nanometers (100–500 nm) of length and 20–60 nm of width. Thus the findings indicate that the pyrolysis products are obtained from the $((C_4H_9)_4)N)_4W_{10}O_{32}$ microsheets and the synthesized material constitutes nanosized one dimensional tungsten oxide materials. Fig 3.4d displays the SEM image of the WO_3 obtained from the pyrolysis of ammonium paratungstate, $(NH_4)_{10}H_2W_{12}O_{42}.xH_2O$. It can be seen that the material is composed of irregular

12

particles of varying size with plate like morphology. From the SEM analysis, it is clear that rod like morphology can be obtained only when tetrabutylammonium group is present in the precursor compound.
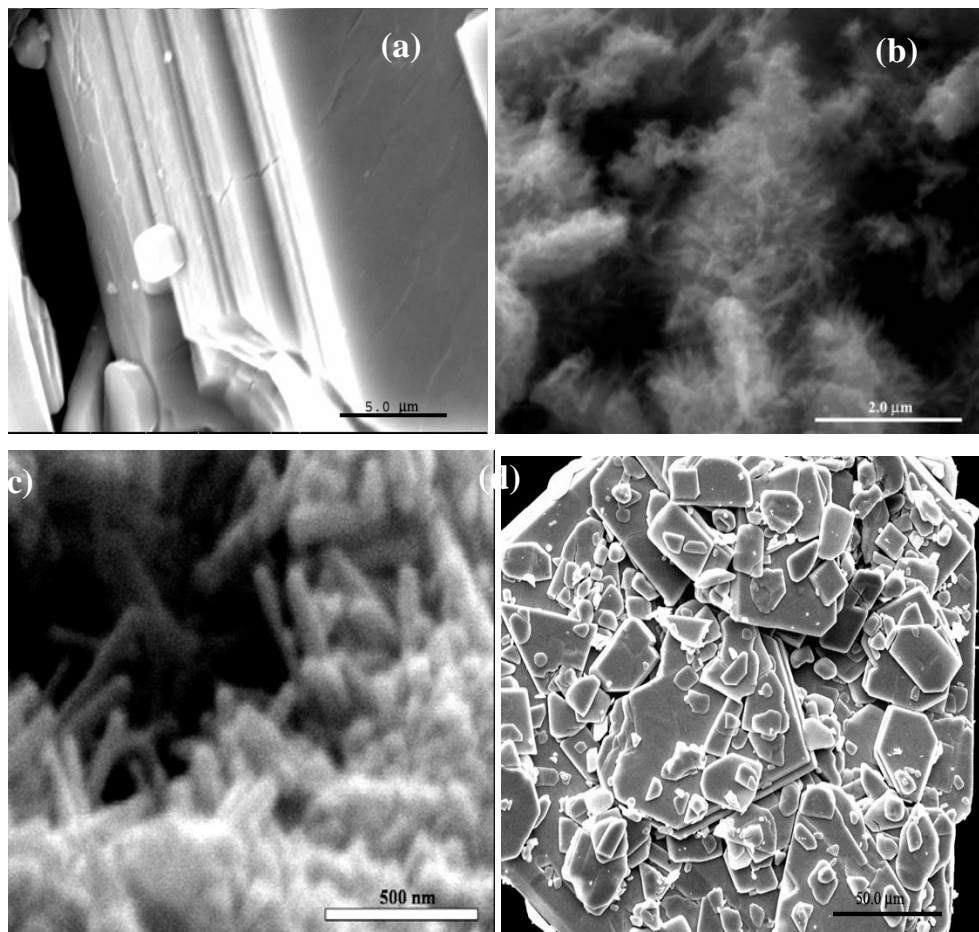
Fig 3. 4 SEM images of (a) $((C_4H_9)_4N)_4W_{10}O_{32})$, (b) and (c) WO_3 nanorods and (d) WO_3 from $(NH_4)_{10}H_2W_{12}O_{42}.xH_2O$

3. 3. 5 TEM and HRTEM measurements

The morphology of WO_3 was further studied by TEM and HRTEM measurements. The TEM image (Fig. 5a) demonstrates the distribution of nanorods in high yields as observed from the SEM. Further, the dimensions of the nanorods calculated from the TEM images vary in the ranges of 130- 480 nm and 18 -56 nm of length and width, respectively. The high resolution TEM image of a nanorod is given in Fig. 3.5b. The lattice fringes calculated are about 0.37 nm and it corresponds to the interplanar

13

spacing of (020) planes of monoclinic WO_3. This observation agrees with the XRD results (JCPDS card no. 75- 2072) and indicates the growth of WO_3 nanorods along (020) plane. The EDAX (Fig.3.6) results confirmed the presence of respective constituent elements in WO_3 nanorods. The copper signals originate from a copper supporting microgrid.
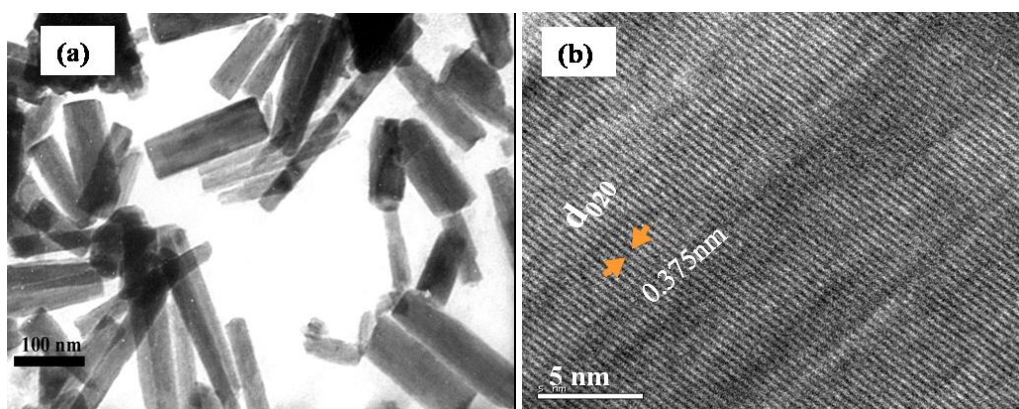
Fig. 3. 5(a) TEM and (b) HRTEM of WO_3 nanorods
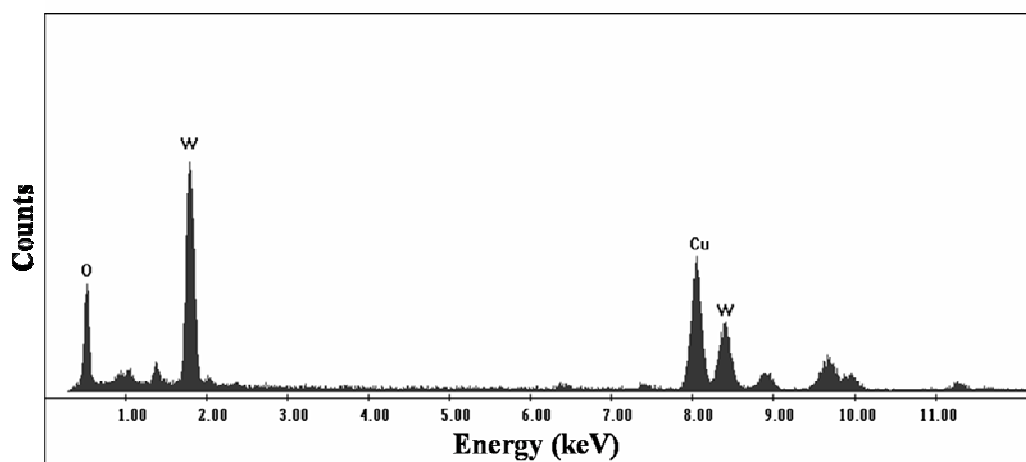
Fig. 3. 6 EDX of WO_3 nanorods

3.3.6 Scheme for the formation of WO₃ nanorods

A schematic representation of the formation of WO_3 nanorods is shown in Scheme.3.1. It shows the possible mechanism of tungsten trioxide nanorods formation. The precursor material is composed of the cationic surfactant group (tetrabutyl ammonium ion) and the anionic decatungstate ion, represented as octahedral units (Chemseddine *et al.*, 1984). Formation of the precursor can be understood as follows: TBA^+ cations react with the tungsten oxide octahedra (Scheme 3.1a) and forms lamellar aggregates (also supported from the SEM image Fig 3.4a) of the $((C_4H_9)_4N)_4W_{10}O_{32}$ in which the tungstate anions are encapsulated in the array of TBA groups. The TBA groups are suggested to behave as glue that holds the WO_6 octahedra together with spacing between different lamellar layers (Scheme 3.1b). In the crystallization process, surfactant molecules may serve as growth controllers, as well as agglomeration inhibitors, by forming an encapsulated layer. When heated at 450 °C for 2h, the structure directing, tetrabutylammonium group decomposes resulting in the formation of nanorods of WO_3 (Scheme 3.1c). The presence of tetrabutylammonium group in the precursor plays a vital role in the formation of nanorods. The hydrophilic head group of the surfactant binds to the $W_{10}O_{32}^{4-}$ anions. During this process the hydrophobic tail groups form a shield outside the anionic octahedra which prevents their agglomeration. The presence of the surfactant coating is of key importance not only for hydrophilic stabilization of the octahedra, but also for controlling long range self-assembly in concentrated dispersions.

Scheme. 3. 1 Formation of WO$_3$ nanorods

3.4 Characterization of MoO$_2$ nanorods

3.4.1 X-ray diffraction studies

In Fig.3.7, a representative XRD pattern for the as-synthesized molybdenum oxide nanorods is displayed. All the peaks can be indexed undisputedly to monoclinic MoO$_2$ [JCPDS no. 76-1807]. Diffraction peak of (011) is stronger when compared to all other peaks, indicating that the (011) is the major growth direction.

Fig. 3. 7 XRD of MoO$_2$ nanorods

3.4.2 Transmission Electron microscopic studies

A typical TEM image is shown in Fig.3.8a. The width and length of the nanorods are in the range of 20-50 nm and 5-10 μm, respectively. Fig.3.8b represents the HRTEM image of a single MoO_2 nanorod with well defined lattice fringes. The interplanar spacing, d value calculated from this image is 0.34 nm corresponding to (011) planes of monoclinic MoO_2. The EDX spectrum (Fig.3.9) shows that the nanorods are composed only of Mo and O. Thus the findings indicate that the as-synthesized materials are nanosized one-dimensional molybdenum oxide materials.
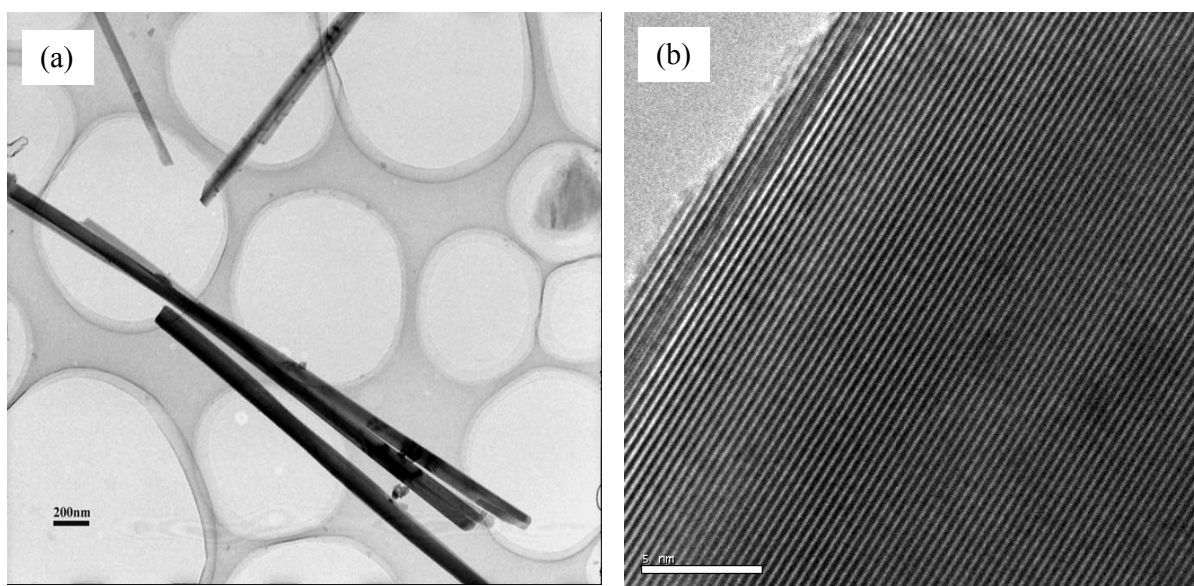
Fig. 3. 8 (a) TEM and (b) HRTEM images of MoO_2 nanorods
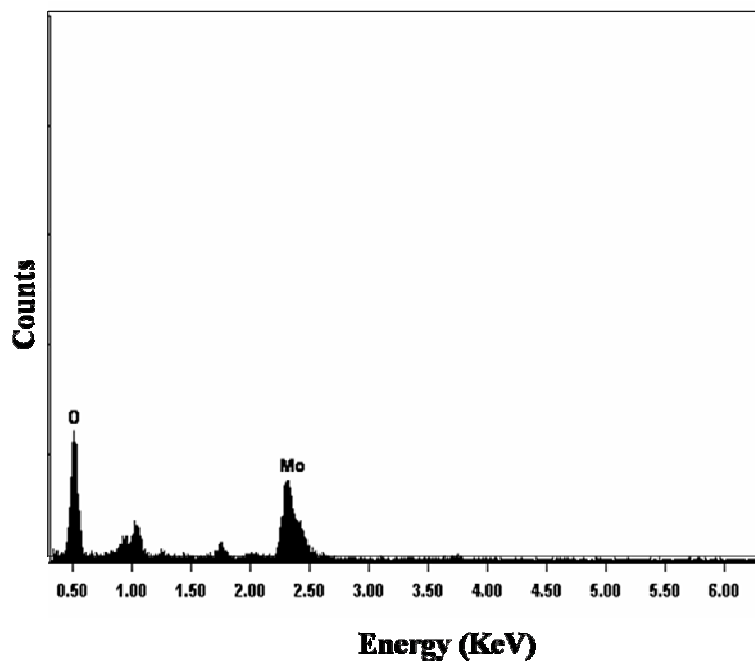
Fig. 3.9 EDX spectrum of MoO$_2$ nanorods

3.4.3 Raman analysis

Raman spectrum of the as-synthesized MoO$_2$ nanorods is given in Fig.3.10 which illustrates the appearance of Raman bands at 748, 582, 498, 468, 370, 230, 208 cm^{-1}. These bands are in good agreement with the reported values for monoclinic MoO$_2$ (Kumari *et al*., 2007).
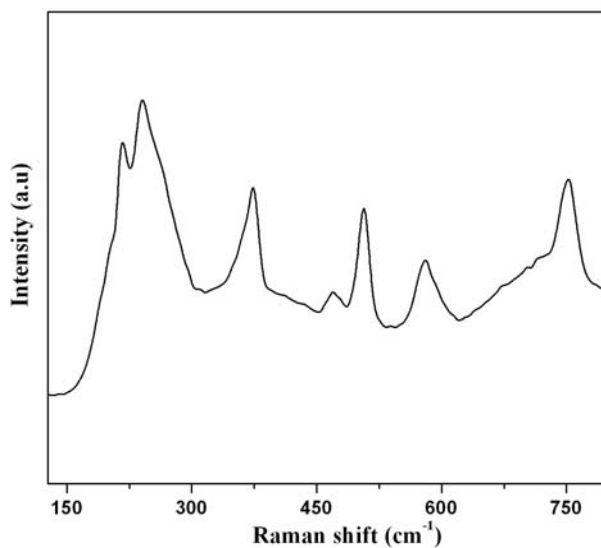
Fig.3.10 Raman spectrum of MoO$_2$ nanorods

3.5 Characterization of Mo$_x$V$_y$O$_z$ nanorods

The mixed oxides containing Mo and V prepared by the thermal decomposition of tetrabutylammonium phosphomolybdovanadate were characterized by powder XRD and electron microscopic studies.

3.5.1 XRD analysis

The XRD pattern of the as-synthesized material is shown in Fig.3.11. These peaks could be indexed to (020), (110), (120), (111), (121), (150), (210) and (002) diffraction planes of a single phase of MoO$_3$ with an orthorhombic crystal structure (JCPDS: 89-5108) and (110), (211), (310) diffraction planes of VO$_2$ (JCPDS: 76-0678) with a tetragonal crystal structure. The (224) peak of MoO$_3$ at 38.97° and (200) peak of VO$_2$ at 39.54° have overlapped to give a broad peak.
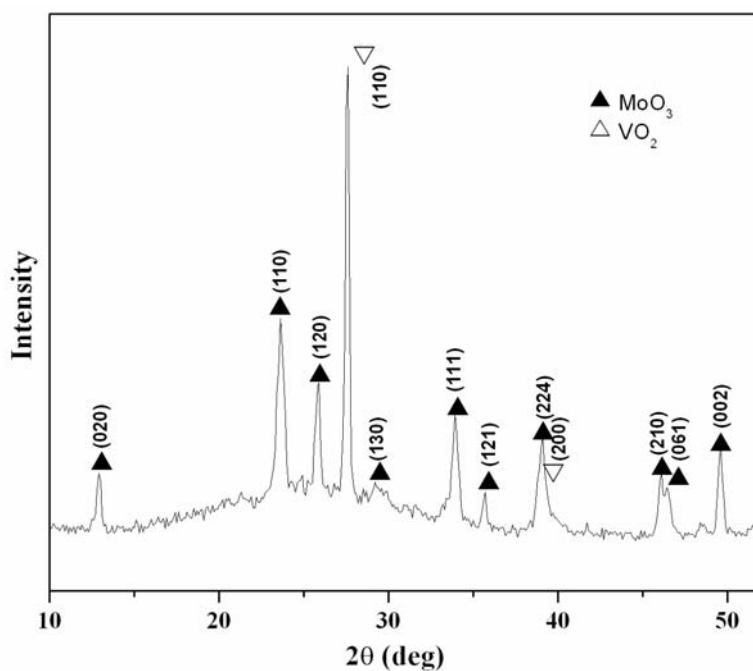
Fig. 3. 11 XRD of Mo$_x$V$_y$O$_z$ nanorods

3.5.2 Electron microscopic studies

SEM image of as synthesized product is presented in Fig.3.12a. The image show that the product consists of bundles of $Mo_xV_yO_z$ nanorods in high yield. The TEM image containing nanorods of 180-266 nm in length and a width of ~23 nm can be seen in Fig.3.12b. The EDAX spectrum (Fig.3.13) shows the peaks corresponding to the constituent elements, Mo, V and O of the nanorods.
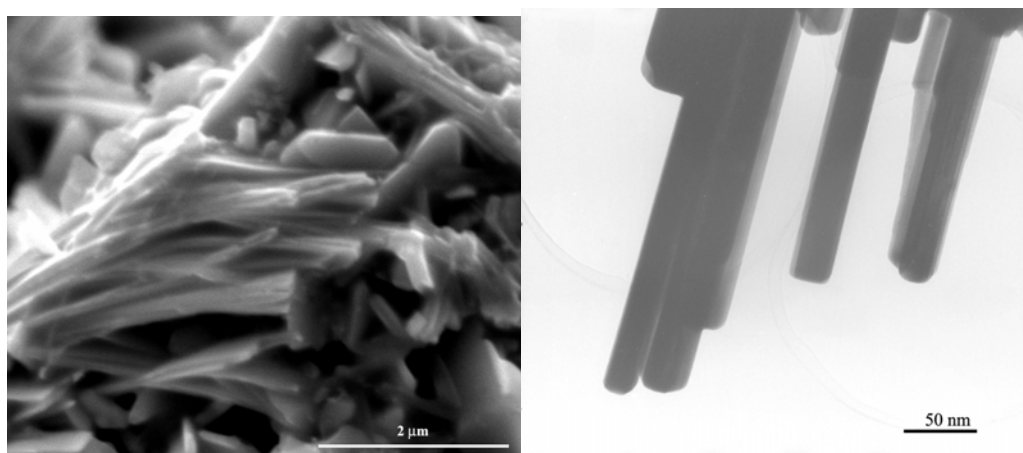
Fig. 3.12 (a) SEM and (b) TEM images of $Mo_xV_yO_z$ nanorods
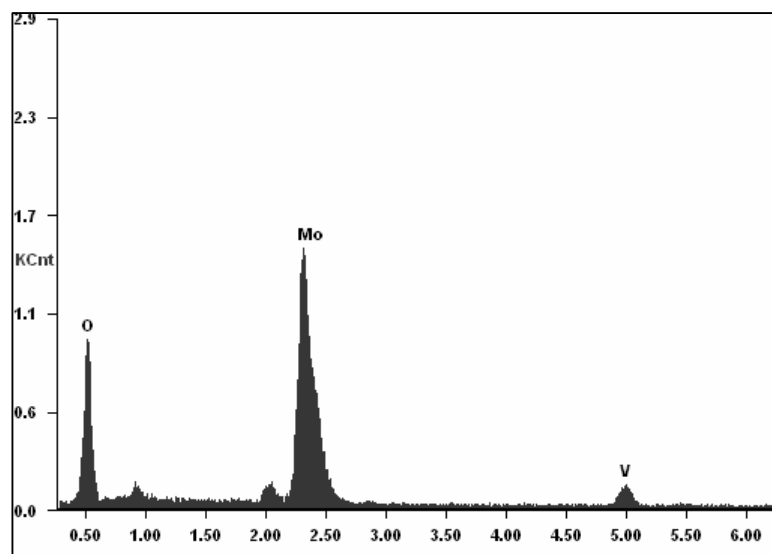
Fig. 3.13 EDX spectrum of $Mo_xV_yO_z$ nanorods

3.6 Characterization of MoS$_2$

3.6.1 X-ray diffraction pattern

Fig.3.14 shows the typical X-ray diffraction (XRD) pattern of the as-synthesized MoS$_2$ nanotubes. It can be observed that all the diffraction peaks in the spectrum can be undisputedly indexed to the pure phase of MoS$_2$ with a rhombohedral structure (JCPDS no: 77 – 0341). The peaks at 33.0° due to the (101) plane and 34.09° due to the (012) plane have overlapped to give a broad peak.
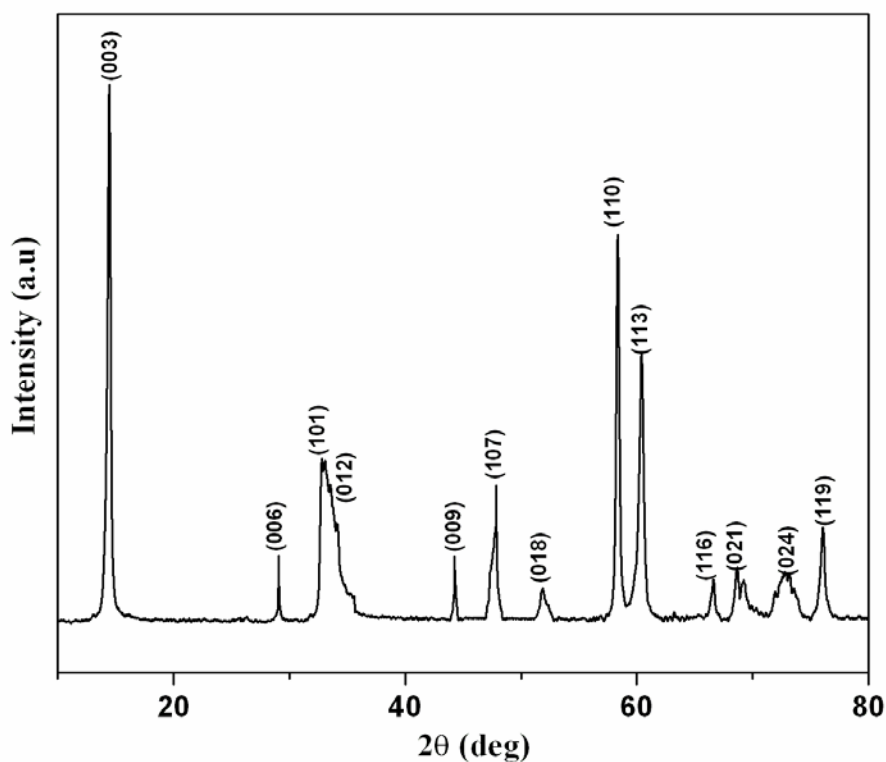
Fig. 3.14 XRD pattern of as-synthesized MoS$_2$

3.6.2 Raman analysis

Raman spectrum of as-synthesized MoS$_2$ is given in Fig.3.15 with the bands at 392 cm^{-1}, 421 cm^{-1} and 464 cm^{-1}. The results obtained are compared with the recent reports on MoS$_2$ nanotubes obtained by Virsek *et al.,* (2007) and the values obtained are in consistent with the reported values. It has been elucidated that the nanotubes

exhibits upshift when compared to the bulk MoS_2. The MoS_2 in the current study too shows an upshift of bands to higher wavenumbers when compared to bulk MoS_2 as observed in the literature.
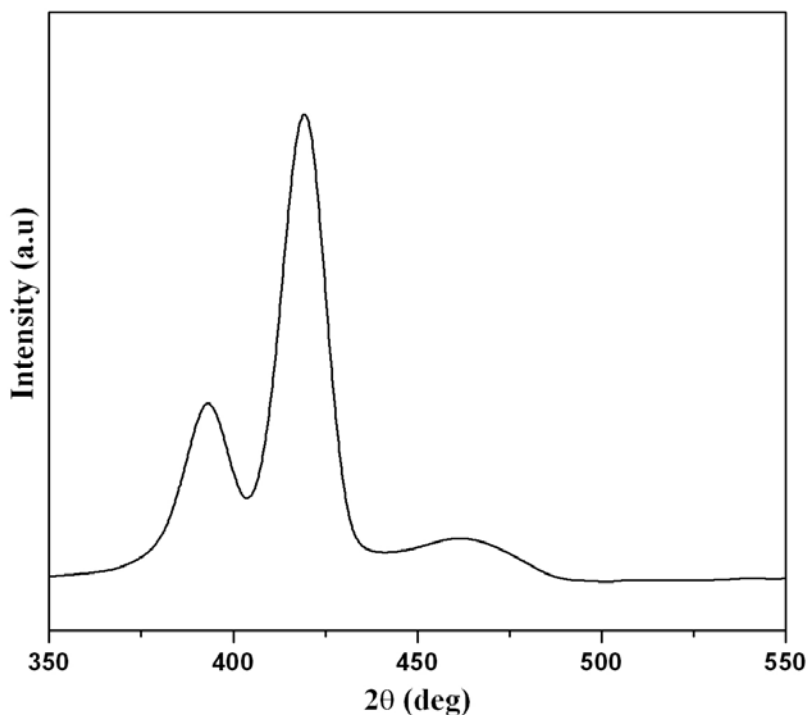
Fig.3.15 Raman spectrum of MoS_2 nanorods

3.6.3 SEM and EDX

Fig.3.16a & b shows the representative scanning electron microscopy images of MoS_2 samples. Fig.3.16a indicates that the as-synthesized MoS_2 have tube like morphology in high yields. A magnified image of Fig.3.16a shows a nanotube of a few micrometers length and a diameter of ~ 75nm with a circular tip, marked with a circle. However, it also shows the presence of nanoparticles along the nanotube. In order to have a clear picture of this, TEM was also employed.
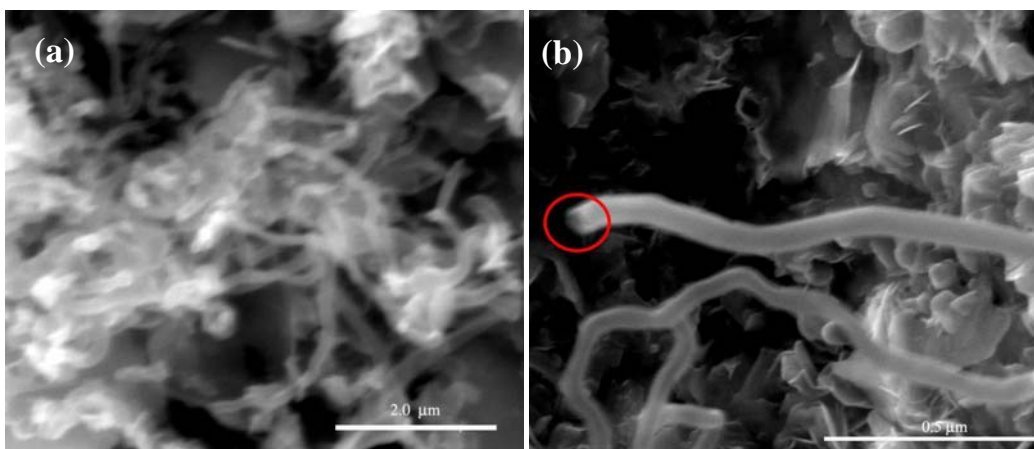
Fig.3.16 (a) & (b) SEM images of as-synthesized MoS$_2$

3.6.4 TEM of MoS$_2$

The TEM images of MoS$_2$ in Fig.3.17a & b show that two types of nanostructures (nanoparticles and nanotubes) are formed. This observation is in consistent with the SEM results (Fig.3.16b) where in, the presence of both nanoparticles as well as nanotubes in the as-synthesized product could be evidenced. There are evidences for the formation of other nanostructures such as nanorods, nanofibers and nanoparticles during the synthesis of nanotubes (Nath *et al*., 2001; Tenne *et al*., 1992; Zelenski and Dorhout, 1998).   In the synthesis that utilizes MoO$_3$ as the precursor compound, MoO$_{3-x}$ is formed as the intermediate during reduction, followed by reaction with H$_2$S to form MoS$_2$.   In the current work, as the thermal decomposition of $((C_4H_9)_4N)_2Mo_6O_{19}$ produces MoO$_2$ directly, we have not provided any reducing atmosphere (forming gas).   It has been shown that the starting material, reaction conditions such as temperature, inert gas to H$_2$ ratio etc., influence the morphology of the products. Fig.3.17a shows the formation of triangular nanoplatelets and MoS$_2$ with an edge length of ~33 nm. Nanoplatets of MoS$_2$ were shown to have a high catalytic activity for hydrodesulfurization (Villarreal *et al*., 2007).   The inset of Fig.3.17a shows the formation of octahedral nanoparticles but the edges are not clear. Polyhedral MoS$_2$ and WS$_2$ (platelets) were also shown to have good potential as solid

state lubricants (Rapport *et al*., 1997). Fig.3.17b is a representative nanotube of molybdenum sulfide with a diameter of ~ 63 nm and a length of more than 555 nm. The tip of the tube, marked by a circle, shows that the nanotube has an open end. Open ended MoS_2 nanotubes find important application in catalysis. Chen *et al* (2002) have shown that open ended MoS_2 nanotubes function effectively as catalysts for the methanation of CO and H_2 at a low temperature. This has lead to the finding that open ended MoS_2 nanotubes can be potential candidate for the conversion of global carbon oxides as well as catalysts for fuel cells to eliminate CO poisoning. Fig.3.17c &d also show the open end of the nanotubes. The nanotubes having a hollow core with an inner diameter of ~ 16 nm and a wall thickness of ~ 20 nm can also be observed. In order to have a clear view of this, HRTEM was also performed.
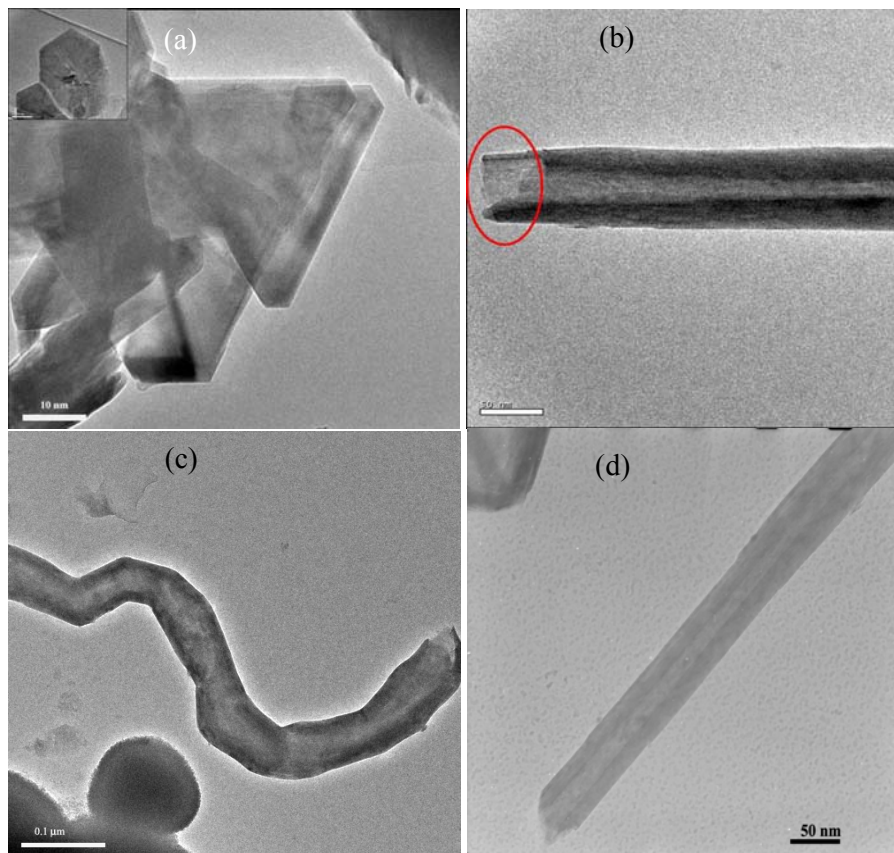
Fig. 3.17 (a), (b), (c) and (d) TEM images of as-synthesized MoS_2

3.6.5 HRTEM and EDX analysis

The high resolution image (Fig.3.18a) reveals that the obtained tubular structures are exclusively multiwalled nanotubes. The outer diameter of the tube is ~ 70 nm with a wall thickness of ~ 16 nm. The image reveals the presence of layers with a spacing of 0.61 nm corresponding to the (003) planes of rhombohedral lattice of MoS_2. This is in good agreement with the value obtained from the XRD data (JCPDS: 77 – 0341). Analysis by energy dispersive X-ray spectroscopy shows the presence of Mo and S in the sample, with an atomic ratio of 1:2, confirming that the as-synthesized nanotubes as well as nanoparticles are only MoS_2.
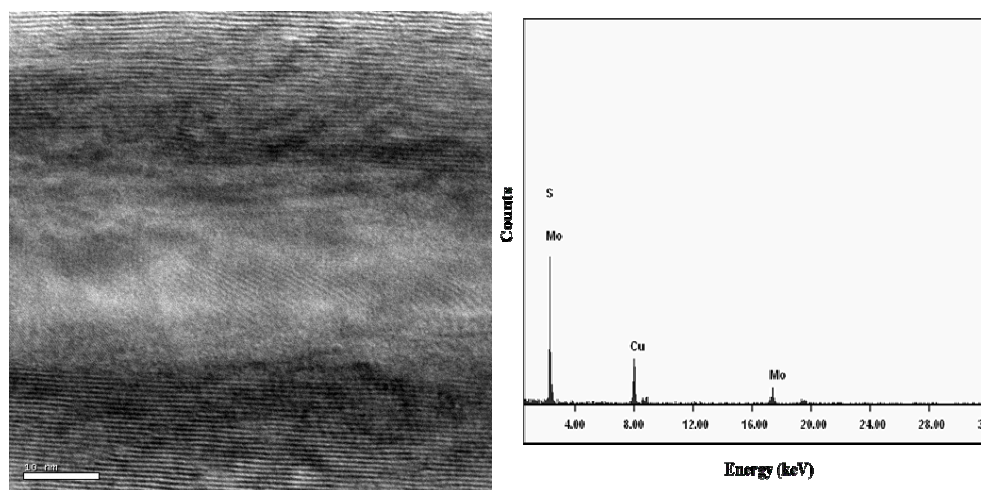
Fig. 3.18 (a) HRTEM and (b) EDX of as-synthesized MoS_2

3.7 Characterization of tungsten sulfide (WS_2)

3.7.1 X-ray diffraction pattern

The X-ray diffraction pattern of the as-synthesized tungsten sulfide is given in Fig.3.19. The material exhibits reflections at planes corresponding to the rhombohedral WS_2 (JCPDS: 35-0651) with the (003) peak being intense among the other peaks. A broad peak at around 39° is due to the overlap of (104) peak at 38.67°

and (015) peak at 41.22°. Similarly the peaks at 48.36° and 51.85° have overlapped to give a broad peak.
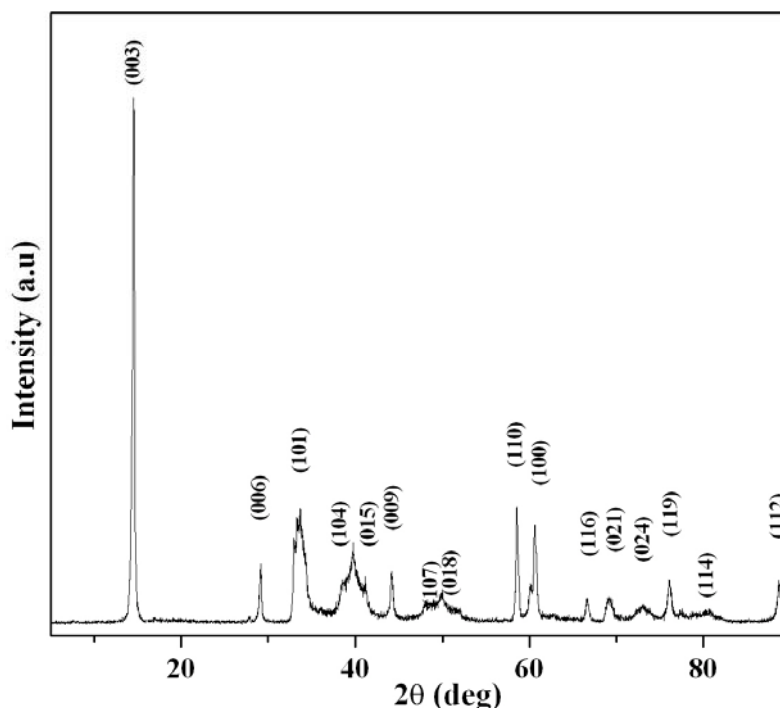
Fig.3.19 XRD pattern of as-synthesized WS_2

3.7.2 SEM and EDX

The SEM image (Fig.3.20a) of the as-synthesized WS_2 shows the presence of shorter nanorods as well as several hexagonal shaped particles. Unlike the other reports wherein nanotubes and fullerene-like nanoparticles of WS_2 were produced, the current method has yielded nanoplatelets of WS_2. In their reports, when started with WO_3, a reduction step is followed to produce WO_{3-x} and then sulfidization has been proceeded to form WS_2. It has been reported that when a reducing atmosphere is not introduced, only platelets of WS_2 are produced (Feldman *et al*., 1998). In the current method, WS_2 is produced from $((C_4H_9)_4N)_4W_{10}O_{32})$ via the formation of WO_3 but still a reduction step was not adopted before sulfidiztion. Hence as reported earlier, only platelets are formed. Nanoplatelets of WS_2 and MoS_2 have been proven experimentally as well as theoretically to have 'metallic-like' character and moreover

26

owing to their stability from energetics point of view, they have been identified as suitable candidates for future nanoelectronics (Seifert *et al*., 2002; Bertram *et al*., 2006). The EDX spectrum (Fig.3.20b) show the signals due to W and S in the 1:2 ratio.
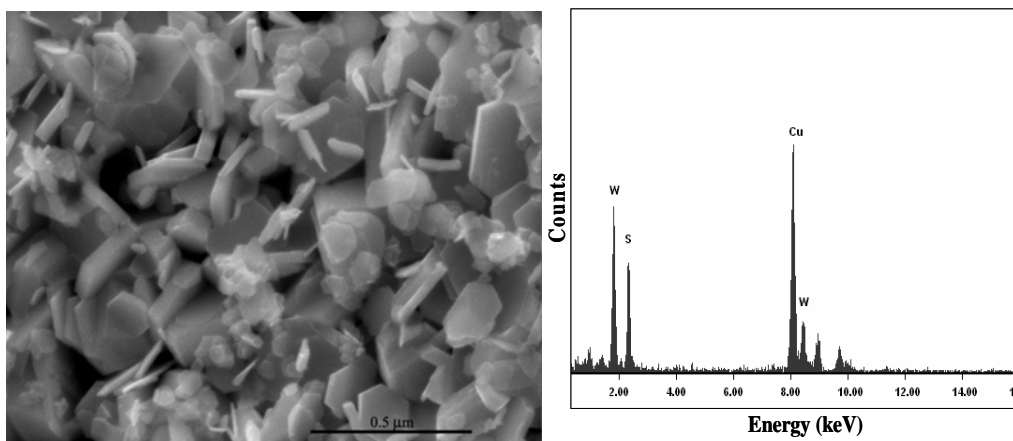
Fig. 3.20 (a) SEM and (b) EDX of as-synthesized WS_2

3.7.3 TEM and HRTEM analysis

The TEM images of the WS_2 at different magnifications are given in Fig.3.21a & b which show the presence of two sort of nanomaterials: (i) short nanorods with dimensions of 20-40 nm in length and 8-20 nm in width and (ii) irregular shaped nanoparticles, closer to spherical shape with a diameter of ~20 nm and a few hexagons. This observation is in consistent with the SEM image of WS_2 (Fig.3.20a). The interplanar spacing, d, calculated from the HRTEM image (Fig.3.21c) is 0.61 nm, which corresponds to the (003) plane of rhombohedral WS_2 (JCPDS: 35-0651).
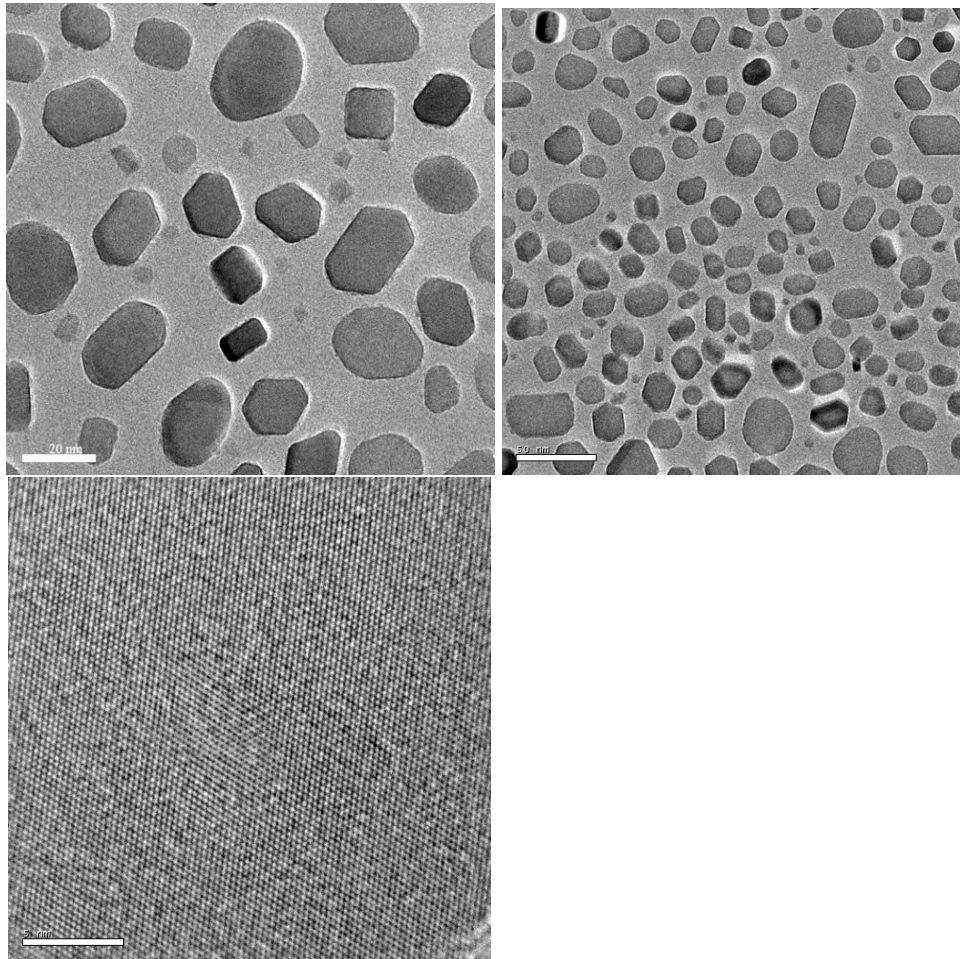
3.8 Summary

A simple and easy method based on thermal decomposition was adopted to fabricate 1-D nanorods of WO_3, MoO_2 and $Mo_xV_yO_z$. The advantage of this method is the tunability of the metal precursor and the surfactant group. This aspect of the method can be exploited for the synthesis of a variety of transition metal oxide nanostructures. Syntheses of MoS_2 and WS_2 nanostructures were carried out by heat treatment of the metal oxide nanorods in H_2S atmosphere at elevated temperature. The electron microscopic images of MoS_2 nanotubes show that they are formed with open ended tips which will make the material an efficient catalyst for various applications.

REFERENCES

1. **Abdullah, S. F., S. Radiman, M. A. Abd. Hamid and N. B. Ibrahim** (2006) Effect of calcination temperature on the surface morphology and crystallinity of tungsten (VI) oxide nanorods prepared using colloidal gas aphrons method. *Coll. Surf. A* **280**, 88- 94.

2. **Baek, Y., Y. Song and K. Yong** (2006) A novel heteronanostructure system; Hierarchical W nanothorn arrays on WO_3 nanowhiskers. *Adv. Mater*. **18,** 3105-3110.

3. **Baek, Y. and K. Yong** (2007) Controlled growth and characterization of tungsten oxide nanowires using thermal evaporation of WO_3 powder. *J. Phys. Chem. C* **111**, 1213- 1218.

4. **Bertram, N., J. Cordes, Y. D. Kim, G. Gantefor, S. Gemming and G. Seifert** (2006) Nanoplatelets made from MoS_2 and WS_2. *Chem. Phys. Lett.* **418**, 36-39.

5. **Bowler, R., T. J. Davies, M. E. Hyde and R. G. Compton** (**2005**) Electrochemical cell for surface analysis. *Anal. Chem.* 77, 1916-1919.

6. **Che, M., M. Fournier and J. P. Launay** (1979) The analog of surface molybdenyl ion in Mo/SiO2 supported catalysts: The isopolyanion $Mo_6O_{19}^{3-}$ studied by EPR and UV-visible spectroscopy. Comparison with other molybdenyl compounds. *J. Chem. Phys*. **71**, 1954-1960.

7. **Chemseddine, A., C. Sanchez, J. Livage, J. P. Launay, M. Fournier** (1984) Electrochemical and photochemical reduction of decatungstate : a reinvestigation. *Inorg. Chem.* **23**, 2609-

8. **Chen, J., S. L. Li, Q. Xu and K. Tanaka** (2002) Synthesis of open-ended MoS2 nanotubes and the application as the catalyst for methanation. *Chem. Commun.* 1722 -1723.

9. **Cheng, F., J. Chen and X. Gou** (2006) MoS_2-Ni nanocomposites as catalysts for hydrodesulfurization of thiophene and thiophene derivatives. *Adv. Mater.* **18**, 2561-2564.

10. **Cheng, F. and J. Chen** (2006) Storage of hydrogen and lithium in inorganic nanotubes and nanowires. *J. Mater. Res*. **21**, 2744-2757.

11. **Choi, H. G., Y. H. Jung and D. K. Kim** (2005) Solvothermal synthesis of tungsten oxide nanorod/nanowire/nanosheet.*J. Am. Ceram. Soc.* **88**, 1684-1686.

12. **Dominko, R., M. Gaberscek, D. Arcon, A. Mrzel, M. Remskar, D. Mihailovic, S. Pejovnik, J. Jamnik** (2003) Electrochemical preparation and characterization of Li_zMoS_{2-x} nanotubes. *Electrochim. Acta* **48**, 3079-3084.

13. **Feldman,Y., E. Wasserman, D. J. Srolovitz and R. Tenne** (1995) High-rate, gas phase growth of MoS2 nested inorganic fullerenes and nanotubes. *Science* **267,** 222-225.

14. **Feldman, Y., G. L. Frey, M. Homyonfer, V. Lyakhovitskaya, L. Margulis, H. Cohen, G. Hodes, J. L. Hutchinson and R. Tenne** (1996) Bulk synthesis of inorganic fullerene like MS_2 from the respective trioxides and the reaction mechanism,

15. **Feldman, Y., V. Lyakhovitskaya and R. Tenne** (1998) Kinetics of nested inorganic fullerene-like nanoparticle formation. *J. Am. Chem. Soc.* **120**, 4176-4183.

16. **Gillet, M., R. Delamare and E. Gillet** (2005a) Growth of epitaxial tungsten oxide nanorods. *J. Crystal Growth* **279**, 93 -99.

17. **Gillet, M., R. Delamare and E. Gillet** (2005b) Growth, structure and electrical properties of tungsten oxide nanorods. *Eur. Phys. J. D* **34**, 291- 294.

18. **Gloskovskii, A., S. A. Nepijko, M. Cinchetti and G. Schonhense, G. H. Fecher, H. C. Kandpal, C. Felser, H. A. Therese, N. Zink and W. Tremel** (2006) Time-of-flight photoelectron spectromicroscopy of single MoS_2 nanotubes. *J. Appl. Phys.* **100**, 0843301-0843301.

19. **Gu, G., B. Zheng, W. Q. Han, S. Roth and J. Liu** (2002) Tungsten oxide nanowires on tungsten substrates. *Nano Lett*. **2**, 849- 851.

20. **Gu, Z., T. Zhai, B. Gao, X. Sheng, Y. Wang, H. Fu, Y. Ma and J. Yao** (2006) Controllable assembly of WO_3 nanorods/nanowires into hierarchical nanostructures. *J. Phys. Chem. B* **110**, 23829- 23836.

21. **Guo, D. Z., K. Y. Zhang, A. Gloter, G. M. Zhang and Z. Q. Xue** (2004) Synthesis and characterization of tungsten oxide nanorods. *J. Mater. Res.* **19**, 3665- 3670.

22. **Klinke, C., J. B. Hannon, L. Gignac, K. Reuter and P. Avouris** (2005) Tungsten oxide nanowire growth by chemically induced strain. *J. Phys. Chem. B* **109**, 17787- 17790.

23. **Koltypin, Y., S. I. Nikitenko and A. Gedanken** (2002) The sonochemical preparation of tungsten oxide nanoparticles. *J. Mater. Chem.* **12**, 1107- 1110.

24. **Kumari, L., Y. R. Ma, C. C. Tsai, Y. W. Lin, S. Y. Wu, K. W. Cheng and Y. Liou** (2007) X-ray diffraction and Raman scattering studies on large-area array and nanobranched structure of 1D MoO_2 nanorods. *Nanotechnology* **18** 115717(1) – 115717(8).

25. **Lakshmi, B. B., P. K. Dorhout and C. R. Martin** (1997) Sol-gel template synthesis of semiconductor nanostructures. *Chem. Mater.* **9**, 857- 862.

26. **Lavayen, V., N. Mirabal, C. O. Dwyer, M. A. Santa Ana, E. Benavente, C. M. Sotomayor Torres and G. Gonzalez** (2007) The formation of nanotubes and nanocoils of molybdenum disulphide. *Appl Surf Sci.* **253**, 5185 – 5190.

27. **Lee, K., W. S. Seo and J. T. Park** (2003) Synthesis and optical properties of colloidal tungsten oxide nanorods. *J. Am. Chem. Soc.* **125**, 3408- 3409.

28. **Li, Y., X. Li, Z. X. Deng, B. Zhou, S. Fan, J. Wang and X. Sun** (2002) From surfactant-inorganic mesostructures to tungsten nanowires. *Angew. Chem. Int. Ed.* **41**, 333- 335.

29. **Li, X. L., J. F. Liu and Y. D. Li** (2003) Large scale synthesis of tungsten oxide nanowires with high aspect ratio. *Inorg. Chem.* **42**, 921-924.

30. **Li, Y., Y. Bando and D. Golberg** (2003a) Quasi- aligned single-crystalline $W_{18}O_{49}$ nanotubes and nanowires. *Adv. Mater.* **15**, 1294- 1296.

31. **Li, Y., Y. Bando, D. Golberg and K. Kurashima** (2003b) WO_3 nanorods/nanobelts synthesized via physical vapor deposition process. *Chem. Phys. Lett.* **367**, 214- 218.

32. **Liang, Y., Z. Yi, X. Lei, X. Ma, S. Yang, J. Sun, L. Yuan and Y. Zhou** (2006a) A novel route to prepare nano-sized MoO_2 powders in various dimensions. *J. Alloys Comp.* **421**, 133-135.

33. **Liang, Y., Z. Yi, S. Yang, L. Zhou, J. Sun, Y. Zhou** (2006b) Hydrothermal synthesis and lithium-intercalation properties of MoO_2 nano-particles with different morphologies. *Solid State Ionics* **177**, 501-505.

34. **Liao, C. C., F. R. Chen and J. J. Kai** (2006) WO_{3-x} nanowires based electrochromic devices. *Sol. Energy Mater. Solar Cells* **90,** 1147- 1155.

35. **Liu, Z. W., Y. Bando and C. C. Tang** (2003) Synthesis of tungsten oxide nanowires. *Chem. Phys. Lett.* **372**, 179- 182.

36. **Liu, J., Z. Zhang, C. Pan, Y. Zhao, X. Su, Y. Zhao and D. Yu** (2004) Enhanced field emission properties of MoO_2 nanorods with controllable shape and orientation. *Mater. Lett.* **58**, 3812–3815.

37. **Lou, X. W. and H. C. Zeng** (2003) An inorganic route for controlled synthesis of $W_{18}O_{49}$ nanorods and nanofibers in solution. *Inorg. Chem.* **42,** 6169- 6171.

38. **Lou, X. W. and H. C. Zeng** (2002) Hydrothermal synthesis of α-MoO_3 nanorods via acidification of ammonium heptamolybdate tetrahydrate. *Chem. Mater.* **14**, 4781-4789.

39. **Ma, Y. R., C. C. Tsai, S. F. Lee, K. W. Cheng** (2006) Magnetic materials of large-area one- dimensional WO_2 and MoO_2 nanorods. *J. Mag. Mag. Mater.* **304,** e13–e15.

40. **Margulis, L., G. Salitra, R. Tenne and M. Tallanker** (1993) Nested fullerene like structures. *Nature* 365, 113-114.

41. **Nath, M., Govindaraj, A. and C. N. R. Rao** (2001) Simple synthesis of MoS_2 and WS_2 nanotubes. *Adv. Mater.* **13**, 283-286.

42. **Nomiya, K., K. Yagishita, Y. Nemoto, T. Kamataki** (1997) Functional action of Keggin-type mono-vanadium(V) –substituted heteropolymolybdate as a single species on catalytic hydroxylation of benzene in the presence of hydrogen peroxide. *J. Mol. Catal. A* **126**, 43-53.

43. **Park, B. and K. Yong** (2005) Synthesis and characterization of tungsten oxide nanorods. *Surf. Rev. Lett.* **12**, 745- 748.

44. **Pol, S. V., V. G. Pol, V. G. Kessler, G. A. Seisenbaeva, M. Sung, S. Asai and A. Gedanken** (2004) The effect of a magnetic field on a RAPET (Reaction under Autogenic Pressure at Elevated Temperature) of $MoO(OMe)4$: Fabrication of MoO_2 nanoparticles coated with carbon or separated MoO_2 and carbon particles. *J.Phys.Chem.B* **108,** 6322- 6327.

45. **Pol, S. V., V. G. Pol, G. A. Seisenbaeva, L. A. Solovyov and A. Gedanken** (2005) Synthesis of WO_3 nanorods by reacting $WO(OMe)_4$ under autogenic pressure at elevated temperature followed by annealing. *Inorg. Chem.* **44,** 9938- 9945.

46. **Polleux, J., N. Pinna, M. Antonietti and M. Niederberger** (2005) Growth and assembly of crystalline tungsten oxide nanostructures assisted by bioligation. *J. Am. Chem. Soc.* **127**, 15595.

47. **Polleux, J., A. Gurlo, N. Barsan, U. Weimar, M. Antonietti and M. Niederberger** (2006) Template free synthesis and assembly of single-crystalline tungsten oxide nanowires and their gas sensing properties. *Angew. Chem. Int. Ed.* **45**, 261- 265.

48. **Rapoport, L., Yu. Bilik, Y. Feldman, M. Homyonfer S. R. Cohen and R. Tenne** (1997) Hollow nanoparticles of WS_2 as potential solid state lubricants. *Nature* **387**,791-793.

49. **Rapport, L., N. Fleischer and R. Tenne** (2005) Applications of WS_2 (MoS_2) inorganic nanotubes and fullerene-like nanoparticles for solid lubrication and for structural nanocomposites. *J. Mater. Chem.* **15**, 1782-1788.

50. **Remskar, M., Z. Skraba, F. Cleton, R. Sanjines and F. Levy** (1996) MoS_2 as microtubes. *Appl. Phys. Lett.* **69**, 351-353.

51. **Remskar, M., A. Mrzel, Z. Skraba, A. Jesih, M. Ceh, J. Demsar, P. Stadelmann, F. Levy, D. Mihailovic** (2001) Self assembly of subnanometer-diameter single-wall MoS_2 nanotubes. **292**, 479-481.

52. **Rothschild, R., S. R. Cohen and R. Tenne** (1999) WS_2 nanotubes as tips in scanning probe microscopy. *Appl. Phys. Lett.* **75**, 4025-4027.

53. **Rothschild, A., J. Sloan and R. Tenne** (2000) Growth of WS_2 nanotubes phases. *J. Amer. Chem. Soc.* **122**, 5169-5179.

54. **Santato, C., M. Odziemkowski, M. Ulmann and J. Augustynski** (2001) Crystallographically oriented mesoporous WO_3 films: Synthesis, characterization and applications. *J. Am. Chem. Soc*. **123**, 10639-10649.

55. **Santiago, P., J. A. Ascencio, D. Mendoza, M. P.Alvarez, A. Espinosa, C. R. Sangerman, P. S. Retchkiman, G. A. C. Bragado and M. J. Yacaman** (2004) Synthesis and structural determination of twisted MoS_2 nanotubes. *Appl. Phys. A* **78**, 513-518.

56. **Satishkumar, B. C., A. Govindaraj, M. Nath and C. N. R. Rao** (2000) Synthesis of metal oxide nanorods using carbon nanotubes as templates. *J. Mater. Chem*. **10**, 2115- 2119.

57. **Seifert, G., T. Kohler and R. Tenne** (2002) Stability of metal chalcogenide nanotubes. *J. Phys. Chem. B* **106**, 2497-2501.

58. **Shankar, N., M. F. Yu, S. P. Vanka and N. G. Glumac** (2006) Synthesis of tungsten oxide (WO_3) nanorods using carbon nanotubes as templates by hot filament chemical vapor deposition. *Mater. Lett*. **60**, 771- 774.

59. **Shingaya, Y., T. Nakayama and M. Aono** (2004) Epitaxial growth of WO_x nanorod array on W (001). *Sci. Tech. Adv. Mater*. **5**, 647- 649.

60. **Srivastava, A. K., S. A. Agnihotry and M. Deepa** (2006) Sol-gel derived tungsten oxide films with pseudocubic triclinic nanorods and nanoparticles.*Thin Solid Films* **515**, 1419- 1423.

61. **Tenne, R., L. Margulis, M. Genut and G. Hodes** (1992) Polyhedral and cylindrical structures of tungsten disulphide. *Nature* **360**, 444-446.

62. **Therese, H. A., J. Li, U. Kolb and W. Tremel** (2005) Facile large scale synthesis of WS$_2$ nanotubes from WO$_3$ nanorods prepared by a hydrothermal route. *Solid State sciences*, *7*, 67-72.

63. **Tian, Y., Y. He and Y. Zhu** (2004) Low temperature synthesis and characterization of molybdenum disulfide nanotubes and nanorods. *Mater. Chem. Phys.* **87**, 87-90.

64. **Tsigdinos, G. A. and C. J. Hallada** (1968) Molybdovanadophosphoric Acids and Their Salts. I. Investigation of Methods of Preparation and Characterization. *Inorg. Chem.* **7**, 437-441.

65. **Villarreal, N. E., R. V. Castillo, D. H. Galvan, A. Camacho and M. J. Yacaman** (2007) Structure and catalytic properties of molybdenum sulfide nanoplatelets. *Appl. Catal. A* **328**, 88-97.

66. **Virsek, M., A. Jesih, I. Milosevic, M. Damnjanovic, M. Remskar** (2007) Raman scattering of the MoS$_2$ and WS$_2$ single nanotubes. *Surf. Sci.* **601**, 2868-2872.

67. **Wang, Q., Z. Wen, Y. Jeong, J. Choi, K. Lee and J. Li** (2006) Li-driven electrochemical properties of WO$_3$ nanorods. *Nanotechnology* **17**, 3116- 3120.

68. **Xiao, Z. L. Zhang, Z. Wang, Q. Lu, X. Tian and H. Zeng** (2007) Low-temperature synthesis and structural characterization of single-crystalline tungsten oxide nanorods. *Mater. Lett.* **61**, 1718- 1721.

69. **Zach, M. P., K. Inazu, K. H. Ng, J. C. Hemminger and R. M. Penner** (2002) Synthesis of molybdenum nanowires with millimeter-scale lengths using electrochemical step edge decoration. *Chem. Mater.* **14**, 3206-3216.

70. **Zach, M. P., K. H. Ng and R. M. Penner** (2000) Molybdenum nanowires by electrodeposition. *Science* **290,** 2120-2123.

71. **Zelenski, C. M. and P. K. Dorhout** (1998) Template synthesis of near monodisperse microscale nanofibers and nanotubules of MoS$_2$. *J.Am.Chem.Soc.* **120**, 734-742.

72. **Zhang, H., M. Feng, F. Liu, L. Liu, H. Chen, H. Gao and J. Li** (2004) Structures and defects of WO_{3-x} nanorods grown by in-situ heating tungsten filament. *Chem. Phys. Lett*. **389**, 337- 341.

73. **Zhou, J., N. S. Xu, S. Z. Deng, J. Chen, J. C. She and Z. L. Wang** (2003a) Large-area nanowire arrays of molybdenum and molybdenum oxides : Synthesis and field emission properties. *Adv. Mater*. **15**, 1835-1840.

74. **Zhou, J., N. S. Xu, S. Z. Deng, J. Chen and J. C. She** (2003b) Synthesis of large- scaled MoO_2 nanowire arrays. *Chem. Phys. Lett.* **382**, 443–446.